



# Switchable ferroelectric diode and photovoltaic effects in polycrystalline BiFeO<sub>3</sub> thin films grown on transparent substrates

Yong Zhou<sup>a,b</sup>, Can Wang<sup>a,b,c,\*</sup>, Shilu Tian<sup>a</sup>, Xiaokang Yao<sup>a,b</sup>, Chen Ge<sup>a</sup>, Er-Jia Guo<sup>a,d</sup>, Meng He<sup>a</sup>, Guozhen Yang<sup>a,b</sup>, Kuijuan Jin<sup>a,b,c,\*</sup>

<sup>a</sup> Beijing National Laboratory for Condensed Matter Physics, Institute of Physics, Chinese Academy of Sciences, Beijing 100190, China

<sup>b</sup> University of Chinese Academy of Sciences, Beijing 100049, China

<sup>c</sup> Songshan Lake Materials Laboratory, Dongguan, Guangdong 523808, China

<sup>d</sup> Center of Materials Science and Optoelectronics Engineering, University of Chinese Academy of Sciences, Beijing 100049, China

## ARTICLE INFO

### Keywords:

Polarization switching  
Polycrystalline thin film  
Bismuth iron oxide  
Transparent substrate  
Ferroelectric switchable diode  
Ferroelectric photovoltaic effect  
Pulsed laser deposition

## ABSTRACT

Switchable ferroelectric diode and photovoltaic effects in epitaxial BiFeO<sub>3</sub> (BFO) thin films have drawn intense attention for its potential applications in resistive memory and solar cell. However, both of these two effects were observed almost entirely in epitaxial BFO thin films or bulk crystal. In this paper, we demonstrate these effects in a polycrystalline BFO thin film grown on a transparent Indium Tin Oxide (ITO) covered quartz plate by the pulsed laser deposition technique. The BFO thin film shows good ferroelectricity with remanent polarization of around 60  $\mu\text{C}/\text{cm}^2$  and has a direct band gap of 2.64 eV. The current-voltage curves measured at an Au/BFO/ITO configuration show diode-like rectifying characteristics, and the diode polarity can be reversed with polarization switching. The polycrystalline BFO thin film also exhibits a switchable photovoltaic effect with an open-circuit voltage of approximately 0.2 V and a short-circuit current of nearly 60  $\mu\text{A}/\text{cm}^2$  under illumination. This study demonstrates that the polycrystalline BFO thin film on a transparent substrate also has the ferroelectric switchable diode and photovoltaic effects. Therefore, these results will be useful to expand the application of BFO thin films in optoelectronic devices.

## 1. Introduction

BiFeO<sub>3</sub> (BFO) as a well-known room-temperature multiferroic material possesses strong ferroelectricity and G-type anti-ferromagnetism simultaneously with high Curie temperature ( $T_C = 1100$  K) and Neel temperature ( $T_N = 640$  K) [1, 2]. It has been extensively studied in the past decade due to its interesting physical properties and potential applications in functional devices such as magnetoelectric devices [3–5], nonvolatile memories [6, 7], solar cells [8, 9]. Especially, the ferroelectric switchable diode and photovoltaic effects reported in BFO crystal or epitaxial thin films have attracted much attention [10–15]. These effects were firstly reported by Choi et al. [10] in a BFO bulk crystal. They observed the diode-like rectifying characteristics and the associated photovoltaic effect, and the forward direction of the diode can be reversed with the polarization switching. Subsequently, the ferroelectric switchable diode and resistive switching behaviors were observed in epitaxial BFO thin films, and the origin mechanisms of polarization modulated Schottky barriers were further proposed [12, 13]. Since then, a lot of studies have been carried out on the switchable

ferroelectric diode and photovoltaic effects in epitaxial BFO thin films [9, 11, 16–20]. In a Pt/BFO/SrRuO<sub>3</sub> capacitor structure, the ferroelectric depolarization field in the BFO thin film can drive the electron carriers close to one of the interfaces, which results in a band bending and the corresponding variation of potential barriers at the interfaces. In addition, the depolarization field may also effectively separate the photogenerated electron-hole pairs and leads to a substantial bulk photovoltaic effect, which is distinguished from the conventional photovoltaic effect in p-n junctions where the driving force for charge separation is arising from the built-in field in the very thin depletion layer at the junctions [21]. Thus, much higher open-circuit voltage ( $V_{OC}$ ) and photovoltaic efficiency can be expected in ferroelectrics due to the bulk effect of charge separation. Besides the depolarization field and interface potential barrier, Yang et al. [16] proposed that the electrostatic potential steps at the ferroelectric domain walls also have a significant effect on the separation of the photo-generated carrier. They observed a distinct photovoltaic response in epitaxial BFO thin films with ordered domain patterns at the different electrode and domain wall configurations. Moreover, photoconductivity [22], photoluminescence [23], and

\* Corresponding authors at: Beijing National Laboratory for Condensed Matter Physics, Institute of Physics, Chinese Academy of Sciences, Beijing 100190, China.  
E-mail addresses: [canwang@iphy.ac.cn](mailto:canwang@iphy.ac.cn) (C. Wang), [kjjin@iphy.ac.cn](mailto:kjjin@iphy.ac.cn) (K. Jin).

<https://doi.org/10.1016/j.tsf.2020.137851>

Received 3 August 2019; Received in revised form 28 January 2020; Accepted 6 February 2020

Available online 08 February 2020

0040-6090/© 2020 Elsevier B.V. All rights reserved.

switchable photovoltaic effect [24, 25] of polycrystalline BFO thin films have been reported. However, the switchable diode and photovoltaic effects were observed almost entirely in epitaxial thin films or bulk crystals, and very few studies were performed on BFO thin films with transparent substrates. The studies on BFO thin films using transparent substrates have been reported mainly about the ferroelectricity and optical properties of the films [26, 27]. The ferroelectric switchable diode and the photovoltaic effect have not yet been reported in polycrystalline BFO thin films on transparent substrates.

In this paper, we report the fabrication of a polycrystalline BFO thin film on the transparent ITO/quartz substrate (ITO, Indium Tin Oxide) and the observation of ferroelectric switchable diode and photovoltaic effects in the polycrystalline BFO thin film. The using of transparent substrates might be the requirement for designing photodetectors or solar cells on account of light absorption, and the growth of polycrystalline BFO thin films on commercial transparent substrates is much easier and more economical than epitaxial films. Moreover, the using of polycrystalline thin films may facilitate the integration of BFO with traditional semiconductors [28].

## 2. Experimental procedures

The transparent conductive ITO ( $\text{SnO}_2$ :  $\text{In}_2\text{O}_3$ , 10%:90%) layers and ferroelectric BFO thin films were deposited in sequence on quartz plates by pulsed laser deposition. A XeCl (308 nm) excimer laser was used at an energy density of  $1.5 \text{ J/cm}^2$  at 4 Hz. The BFO thin films were deposited at  $540^\circ\text{C}$  with the oxygen pressure of 7 Pa. After the growth, the BFO films were annealed in situ for 20 min. Prior to the BFO thin films, the conductive ITO layers serving as the bottom electrodes were deposited at  $540^\circ\text{C}$  under an oxygen pressure of 4 Pa. The thickness of the BFO thin films is approximately 300 nm, and the ITO thin films are around 100 nm with a resistance of less than 200 Ohm. The crystal structure of the thin films was revealed by X-ray diffraction (XRD) measurements on a Rigaku Ultima IV (3 kW) diffractometer using the Cu K $\alpha$  radiation ( $\lambda = 1.5406 \text{ \AA}$ ). Second-harmonic generation (SHG) measurements were carried out in typical reflection geometry [29]. The reflection angle was fixed at  $45^\circ$  and the same as the incidence angle. The generated second-harmonic light field could be decomposed into p-polarized component (p-out) and s-polarized component (s-out). The p-out and s-out intensities were recorded as a function of polarization angle of the incident light, respectively. The polarization angle of the incident light was changed by a rotatable  $\lambda/2$  wave plate. The central wavelength of the incident laser generated from a Ti:Sapphire oscillator is 800 nm with a pulse duration of 120 fs, a repetition of 82 MHz, and a laser power of 70 mW. More details about the SHG measurement can be found in [29].

For electrical measurements, circular Au top electrodes with a diameter of 100  $\mu\text{m}$  and a thickness of 50 nm were deposited on the BFO thin films using a metal shadow mask by thermal evaporation. Ferroelectric hysteresis loops were measured on the capacitor configurations of Au/BFO/ITO using a Precision Work Station ferroelectric tester (Premier II, Radiant Technology) at a virtual ground mode. Atomic force microscope (AFM, Asylum Research, MFP-3D) and Piezoresponse force microscopy (PFM, Asylum Research MFP-3D) were used to measure the surface topography and ferroelectric domain configurations of the BFO thin films. The AFM and PFM images were collected and recorded using Pt coated silicon tips with a nominal spring constant of  $\sim 2 \text{ N/m}$  and a free-state resonance frequency of  $\sim 70 \text{ kHz}$ . Current-voltage (IV) curves were measured using a computer-controlled Keithley 2400 source meter. Photoelectric properties of the BFO thin films were investigated under the illumination of a continuous 375 nm laser (Oxxius, the power range of 0–160 mW).

## 3. Results and discussion

XRD patterns of the BFO and ITO thin films are shown in Fig. 1. In

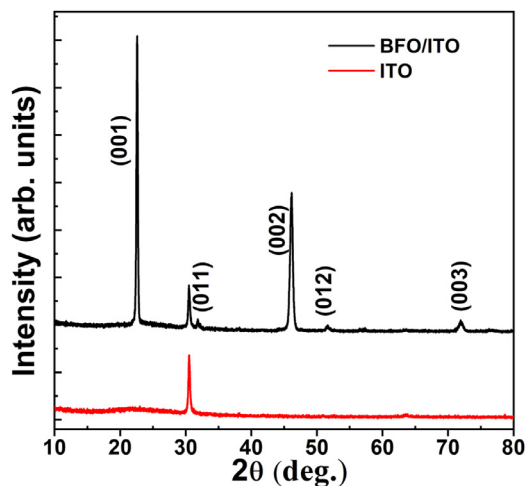


Fig. 1. XRD patterns for the BFO and ITO thin films.

addition to the diffraction peak of ITO, there are several peaks all from BFO thin film, which indicates a polycrystalline structure for the BFO thin film. Both the ITO layer and the BFO layer are highly crystallized without impure parasitic phases such as  $\text{Bi}_2\text{Fe}_4\text{O}_9$  and  $\text{Bi}_{46}\text{Fe}_2\text{O}_{72}$  reported in other studies [30, 31]. The growth process of pure-phase BFO thin films generally needs strict deposition conditions, especially the oxygen pressure and substrate temperature [32, 33]. The parasitic phases always appear in the absence of proper conditions, leading to the degradation of the crystallinity and suppression of the ferroelectricity [34, 35]. Compared with other diffraction peaks, the extremely strong (00l) diffraction peaks indicate that the BFO thin film has a (00l) preferred orientation. For convenience, the pseudo-cubic notation is used here. The BFO thin films with preferred (00l) orientation instead of epitaxy are commonly reported for the films on Pt/Ti/SiO<sub>2</sub>/Si and FTO/glass substrates, which would be caused by the lattice mismatch between the BFO films and substrates [36, 37].

It has been reported that the BFO thin films on ITO show larger strain with a tetragonal structure [27]. However, in this study, the position of the diffraction peaks from the BFO thin film can match very approximately with the standard JCPDS data for bulk BFO, indicating that this BFO film is in a nearly fully relaxed strain state with rhombohedral structure. The relaxed strain state may be related to the existence of grain boundary and its larger thickness. To further reveal the phase structure of the BFO film, Second-harmonic generation (SHG) measurements were carried out in a general reflection geometry as described in detail in Ref. 29. SHG is a useful tool for probing ferroelectricity and determining structural symmetry by modeling of the polarimetry data [38, 39]. SHG intensities as a function of the polarization angle of the incident light, recorded in p-out and s-out configurations, respectively, are shown in Fig. 2(a) and 2 (b), respectively. The observed SHG signal indicates the existence of the ferroelectric phase, while the s-out SHG is twofold rotational symmetry with two major peaks which can be well fitted by using a rhombohedral-like structure. The SHG results don't show the signal of tetragonal structure which is fourfold symmetric with peaks appearing at standard angles of  $45^\circ$ ,  $135^\circ$ ,  $225^\circ$ , and  $315^\circ$  [40], thus this BFO thin film has a rhombohedral-like structure.

Fig. 3 shows the ferroelectric hysteresis loop measured with a frequency of 50 kHz at room temperature for the BFO thin film. The measured polarization at 50 kHz may still have a little bit of contribution from the leakage, but the roughly square-like ferroelectric hysteresis loop suggests good ferroelectricity for the BFO thin film. The observed remanent polarization of the BFO thin film is about  $60 \mu\text{C/cm}^2$  which is comparable to the reported values for epitaxial BFO thin films and larger than the values reported for polycrystalline BFO thin films [36, 41]. Polycrystalline BFO thin films generally show poor

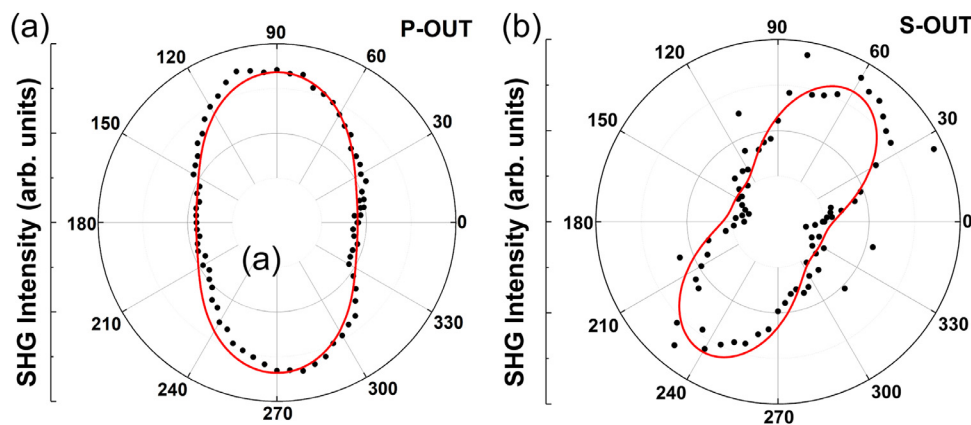


Fig. 2. SHG intensities as a function of polarization angle of the incident light of the BFO thin film, recorded in (a) P-out and (b) S-out configurations, respectively.

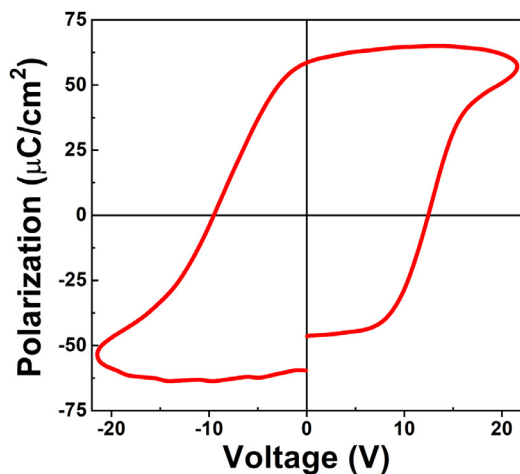


Fig. 3. P-V hysteresis loop of the BFO thin film measured at 50 kHz.

ferroelectricity due to the large leakage current caused by the inner defects and/or parasitic phases [34, 35]. By contrast, our polycrystalline BFO thin film exhibits good ferroelectricity, indicating a high quality of this sample. Moreover, the polarization-voltage loop in Fig. 3 shows a slight shift positively along the voltage axis, suggesting the existence of a built-in electric field in the film. In general, the built-in electric field in ferroelectric films originates from the asymmetric distribution of defect charges and/or free carriers. By high-resolution scanning transmission electron microscopy, Li et al. have revealed that the formation of the defect layers in an insulator can give rise to an inherent built-in electric field [42].

The band gap of the thin film is critically important for the photovoltaic effect and its application. The optical band gap of the BFO thin film was identified through the UV-Visible absorption spectroscopy. Fig. 4(a) plots the absorbance versus wavelength. It can be seen that the BFO thin film mainly absorbs light with a wavelength shorter than  $\sim 500$  nm. As illustrated in Fig. 4(b), the optical band gap of the BFO thin film is calculated to be 2.64 eV through the linear extrapolation of the Tauc's plots  $[(Ah\nu)^2 \text{ vs } h\nu]$  [40, 43]. The obtained band gap value is slightly smaller than the reported value for epitaxial BFO thin films (2.74 eV-2.8 eV) [16, 44], which might be related to the existence of grain boundaries in the polycrystalline thin films.

AFM and PFM measurements were performed to probe the surface morphology and ferroelectric domain structure. Fig. 5(a) shows the surface morphology of the BFO thin film, and the grain size can be roughly estimated to be about several hundred nanometers. The out-of-plane PFM images ( $6 \mu\text{m} \times 6 \mu\text{m}$ ) shown in Fig. 5(b) indicates a preferred downward polarization for the as-grown thin film. The yellow

color represents the polarization pointing upward (from the substrate to the surface) and the violet color represents the polarization pointing downward (from the surface to the substrate). By applying positive or negative voltages on the PFM tip, the ferroelectric domains can be switched. As shown in Fig. 5(b), a  $4 \mu\text{m} \times 4 \mu\text{m}$  square area was electrically written, where the inner area was applied with +20 V and the outer area was applied with -20 V. The distinct contrast between violet and yellow indicate the complete domain switching.

Furthermore, the electrical conductivity and photoelectrical properties of the BFO thin film were measured at as-grown and different polarized states. The upward polarization state or the downward polarization state can be obtained by applying a positive pulse voltage (+8 V for 100 ms) or a negative pulse voltage (-6 V for 100 ms) on the bottom electrode. Fig. 6(a) shows the IV curves measured with sweep voltage of  $\pm 2$  V for the BFO thin film at as-grown, upward polarization, and downward polarization states, respectively. For the as-grown state, the current is small at both positive and negative voltages. However, after electrically poling, the BFO thin film has strikingly different diode-like conduction characteristics. For upward polarization state ( $P_{\text{up}}$ ), the current increases rapidly with positive bias voltage but increases slowly with negative bias voltage, which indicates a forward diode-like behavior. On the contrary, for the downward polarization state ( $P_{\text{down}}$ ), the current shows a reverse diode-like behavior. Thus, the polarity of the rectification characteristics for this polycrystalline BFO thin film can be switched by the polarization reversal. This ferroelectric switchable diode behavior was previously reported only in BFO crystal and epitaxial thin films. The origin of the ferroelectric switchable diode effect has been related to several factors, such as charge injection and trapping [11, 15], the modulated interface Schottky barrier [12, 13], ionic defects and vacancies [14, 45]. In principle, the switchable diode behavior can be explained qualitatively by the polarization modulation of Schottky-like barriers at both the bottom and top electrodes [12].

To describe these mechanisms, by considering the work function of the materials, the energy-band diagrams of Au/BFO/ITO structure are constructed in Fig. 6(b). Here, the BFO thin film is regarded as an n-type semiconductor due to the existence of oxygen vacancies acting as an n-type dopant [46]. A neutral oxygen vacancy ( $V_{\text{o}}$ ) releases one or two electrons to the conduction band (CB) and becomes positively charged ( $V_{\text{o}}^+$  or  $V_{\text{o}}^{2+}$ ). The values of the Schottky barrier height at the BFO/ITO interface and the Au/BFO interface are estimated to be 1.8 eV and 1.5 eV, respectively [shown in Fig. 6b (a')]. For the as-grown state, the Schottky barrier exists at both the top and bottom electrodes, and the BFO capacitor works in a back-to-back diodes' mode [shown in Fig. 6b (b')], thus the current is very small and almost linear with applied bias voltage.

For the electrically polarized states, the depolarization field owing to the incomplete screening of the polarization charge in the BFO thin film can drive the free electrons to neutralize the positive bound

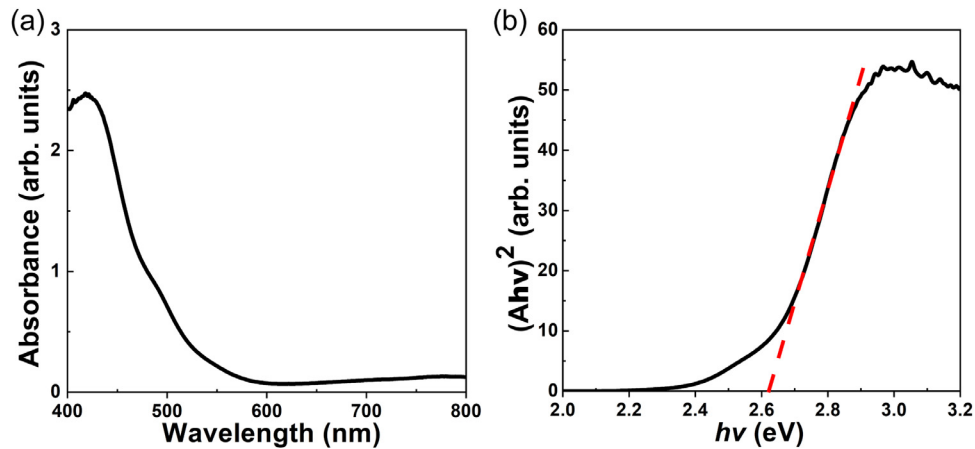


Fig. 4. (a) The UV-Vis absorption spectroscopy results for the BFO thin film. (b) Corresponding the value of the optical band-gap of the film calculated by linear extrapolation (Tauc's plot).

charges and a narrow electron region will form near the interface with positive bound charges, resulting in a downward-bending of the band; meanwhile, another interface with negative bound charges will lose electrons and becomes positively charged, resulting in an upward-bending of the band. The opposite band variations give rise to the modulated Schottky barriers at the two interfaces. Therefore, for the upward polarization state, the built-in potential increases and the depletion region widens; while at the top interface of Au/BFO, the reverse phenomena occur, where the band bending goes down and reaches an ohmic contact. Then, the enhanced Schottky barrier at the bottom interface plays a dominant role in the conduction, thus the capacitor works as a forward diode. And vice versa, for the downward polarization state, the capacitor works as a reverse diode. The enhanced Schottky barrier will contribute to the broadening depletion region at the interfaces. A corresponding built-in electric field ( $E_{bi}$ ) will direct from the depletion region to the negative bound surface charges. Both the ferroelectric depolarization field ( $E_{dep}$ ) and the built-in field ( $E_{bi}$ ) may play an important role to separate the photon-generated carriers for the photovoltaic effect.

The photocurrent characteristics of the Au/BFO/ITO/quartz heterostructure were measured under the illumination of a 375 nm laser with a power density of 630 mW/cm<sup>2</sup>. Fig. 7 shows the IV curves of the BFO thin film at different states (as-grown, upward polarization, and downward polarization). The BFO thin film has remarkably enhanced photovoltaic effect after electrically poling, and the different polarized states correspond to opposite signs of the open-circuit voltage ( $V_{OC}$ ), as well as the short-circuit current ( $I_{SC}$ ). Thus, the photovoltaic effect can also be switched by the electrically induced polarization reversal. The direction of  $I_{SC}$  is always opposite to the diode's forward direction. For the upward polarization state,  $V_{OC}$  and  $I_{SC}$  are around +0.17 V and

−0.61  $\mu$ A/cm<sup>2</sup>, respectively; while for the downward polarization state,  $V_{OC}$  and  $I_{SC}$  are −0.23 V and +57  $\mu$ A/cm<sup>2</sup>, respectively. The small difference of the  $V_{OC}$  for upward polarization state and downward polarization state is due to the different Schottky barrier height. The photovoltaic efficiency of the Au/BFO/ITO/quartz heterostructure at downward polarization is about  $5 \times 10^{-4}\%$  under the illumination of the 375 nm laser, which is higher than that in the epitaxial BFO (001) thin films ( $1.2 \times 10^{-5}\%$ ) [47].

As shown in Fig. 6(b), for the upward polarization state, the Schottky barrier will increase at the BFO/ITO interface and there will form a considerable built-in field ( $E_{bi}$ ) pointing to ITO electrode; while an ohm contact forms at the top interface of Au/BFO. In addition, there is a depolarization field ( $E_{dep}$ ) in the BFO film, which is also pointing to the ITO electrode. Therefore, the total electric field ( $E_{tot}$ ) is decided by  $E_{bi}$  and  $E_{dep}$  ( $E_{tot} = E_{bi} + E_{dep}$ ), which generates a positive photovoltage and a negative photocurrent. In contrast, for the downward polarization state, the Schottky barrier exists at the Au/BFO interface and an ohm contact forms at the bottom interface of BFO/ITO. Meanwhile, the directions of  $E_{bi}$  and  $E_{dep}$  are also reversed to point to the Au electrode, leading to a negative photogenerated open-circuit voltage ( $V_{OC}$ ) and a positive photogenerated short-circuit current ( $I_{SC}$ ). This model is also consistent with the previous reports by Fang et al. and Yuan et al. [18, 46]. To probe the competing role of the interfacial Schottky and bulk polarization effect, systematic poling dependent PV was studied by Swain et al. [48], and they considered that the non-linearity in IV curves reveals a Schottky effect dominant PV response. The observed Schottky-like non-linearity in the IV curves under light illumination suggests that  $E_{bi}$  plays a more important role than  $E_{dep}$ . Therefore, the switchable photovoltaic response in the Au/BFO/ITO sample is mainly attributed to the polarization modulation of Schottky

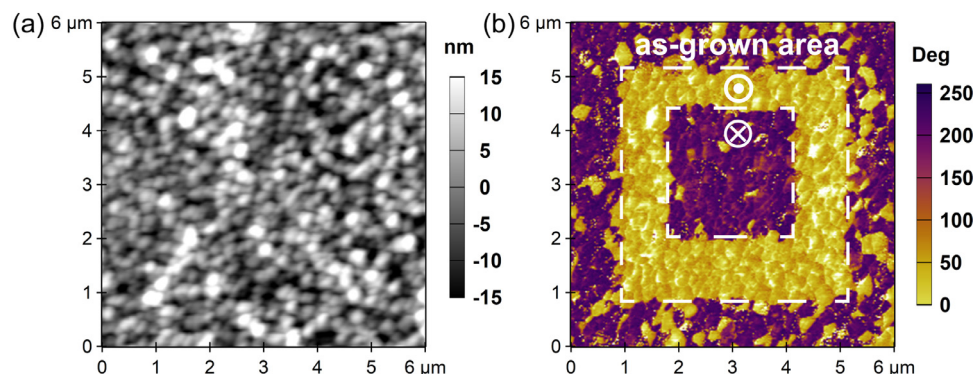
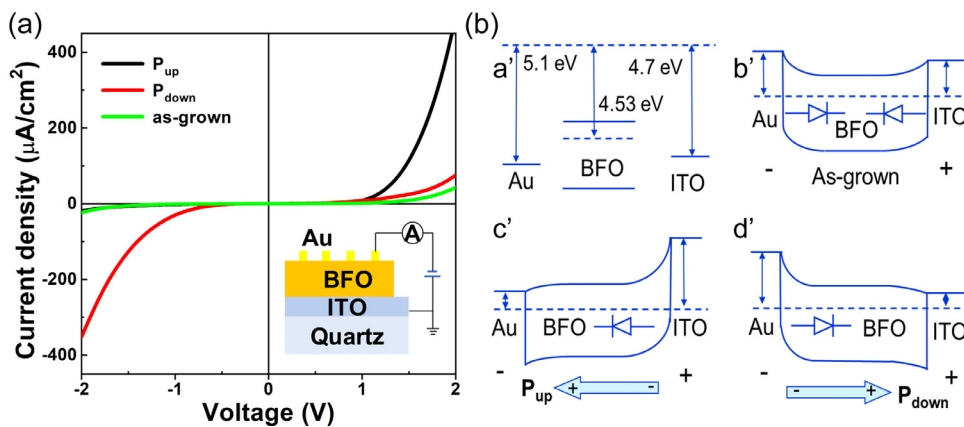
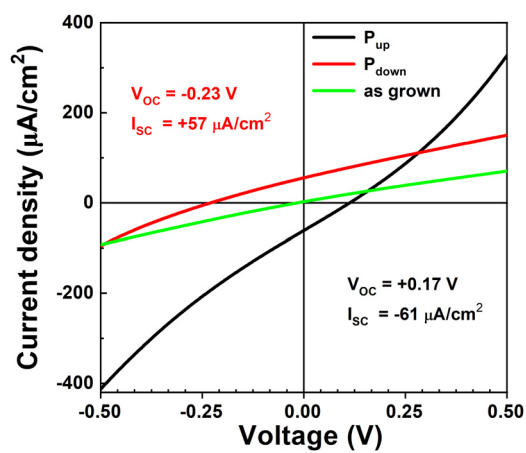


Fig. 5. (a) AFM image of the BFO thin film and (b) the corresponding of out-of-plane PFM written by applying the voltage of  $\pm 20$  V.



**Fig. 6.** (a) IV curves for the BFO thin film at as-grown, upward polarization state ( $P_{up}$ ) and downward polarization state ( $P_{down}$ ). (b) Schematic energy band diagrams illustrating a' the alignment of isolated Au, BFO and ITO; the variations in Schottky barriers from b') the back-to-back diodes as grown to c') a forward diode at  $P_{up}$  and d') a reverse diode at  $P_{down}$ .



**Fig. 7.** IV curves measured under the illumination for the as-grown, upward polarization state ( $P_{up}$ ), and downward polarization state ( $P_{down}$ ).

barriers.

#### 4. Conclusions

Polycrystalline  $\text{BiFeO}_3$  thin films have been grown on transparent substrates using the pulsed laser deposition technique. The polycrystalline BFO thin films show good ferroelectricity with a fully saturated hysteresis loop and a large remanent polarization of  $60 \mu\text{C}/\text{cm}^2$ . It has been demonstrated that the ferroelectric switchable diode and photovoltaic effect can be observed in the polycrystalline  $\text{BiFeO}_3$  thin films. Fabrication of polycrystalline thin films is more cost-efficient compared with that of epitaxy thin film, thus the polycrystalline BFO thin films would have a large possibility for application in the photovoltaic devices and the microelectronic devices.

#### CRediT authorship contribution statement

**Yong Zhou:** Investigation, Resources, Writing - original draft, Writing - review & editing. **Can Wang:** Conceptualization, Methodology, Writing - original draft, Writing - review & editing, Supervision, Project administration, Funding acquisition. **Shilu Tian:** Investigation, Writing - original draft, Writing - review & editing. **Xiaokang Yao:** Investigation, Writing - original draft, Writing - review & editing. **Chen Ge:** Investigation, Writing - original draft, Writing - review & editing. **Er-Jia Guo:** Investigation, Writing - original draft, Writing - review & editing. **Meng He:** Investigation, Writing - original draft, Writing - review & editing. **Guozhen Yang:** Investigation, Writing - original draft, Writing - review & editing. **Kuijuan Jin:** Supervision, Project administration, Funding acquisition.

#### Declaration of Competing Interest

The authors declare that they have no known competing financial interests or personal relationships that could have appeared to influence the work reported in this paper.

#### Acknowledgments

The research was financially supported by National Key R&D Program of China (No. 2019YFA0308500), the National Basic Research Program of China (Grants Nos. 2017YFA0303604), the National Natural Science Foundation of China (Grants Nos. 11874412, 11674385, and 11721404), and the Youth Innovation Promotion Association of CAS (No. 2018008). The authors would like to thank Dr. Hongbao Yao for help with the SHG measurements.

#### References

- [1] I.G. Ismailzade, X-Ray diffractometric determination of the curie temperature and temperature dependence of spontaneous polarization of hexagonal (Rhombohedral) ferroelectrics, *Phys. Status Solidi B* 46 (1971) K39–K41, <https://doi.org/10.1002/pssb.2220460156>.
- [2] G.A. Smolenskii, V.M. Iudin, E.S. Sher, I.E. Stolipin, Antiferromagnetic properties of some perovskites, *Sov. Phys. JETP* 16 (1963) 622.
- [3] J.J. Wang, J.M. Hu, R.C. Peng, Y. Gao, Y. Shen, L.Q. Chen, C.W. Nan, Magnetization reversal by out-of-plane voltage in  $\text{BiFeO}_3$ -based multiferroic heterostructures, *Prog. Rep.* 5 (2015) 10459, <https://doi.org/10.1038/srep10459>.
- [4] N. Ortega, A. Kumar, J.F. Scott, R.S. Katiyar, Multifunctional magnetoelectric materials for device applications, *J. Phys. Condens. Matter* 27 (2015) 504002, <https://doi.org/10.1088/0953-8984/27/50/504002>.
- [5] J. Wu, Z. Fan, D. Xiao, J. Zhu, J. Wang, Multiferroic bismuth ferrite-based materials for multifunctional applications: ceramic bulks, thin films and nanostructures, *Prog. Mater. Sci.* 84 (2016) 335–402, <https://doi.org/10.1016/j.pmatsci.2016.09.001>.
- [6] R. Guo, L. You, Y. Zhou, Z.S. Lim, X. Zou, L. Chen, R. Ramesh, J. Wang, Non-volatile memory based on the ferroelectric photovoltaic effect, *Nat. Commun.* 4 (2013) 1990, <https://doi.org/10.1038/ncomms2990>.
- [7] J.F. Scott, C.A. Paz de Araujo, Ferroelectric memories, *Science* 246 (1989) 1400–1405, <https://doi.org/10.1126/science.246.4936.1400>.
- [8] R. Nechache, C. Harnagea, S. Li, L. Cardenas, W. Huang, J. Chakrabarty, F. Rosei, Bandgap tuning of multiferroic oxide solar cells, *Nat. Photonics* 9 (2014) 61–67, <https://doi.org/10.1038/nphoton.2014.255>.
- [9] M. Alexe, D. Hesse, Tip-enhanced photovoltaic effects in bismuth ferrite, *Nat. Commun.* 2 (2011) 256, <https://doi.org/10.1038/ncomms1261>.
- [10] T. Choi, S. Lee, Y.J. Choi, V. Kiryukhin, S.W. Cheong, Switchable ferroelectric diode and photovoltaic effect in  $\text{BiFeO}_3$ , *Science* 324 (2009) 63–66, <https://doi.org/10.1126/science.1168636>.
- [11] Z. Fan, H. Fan, Z.X. Lu, P.L. Li, Z.F. Huang, G. Tian, L. Yang, J.X. Yao, C. Chen, D.Y. Chen, Z.B. Yan, X.B. Lu, X.S. Gao, J.M. Liu, Ferroelectric diodes with charge injection and trapping, *Phys. Rev. Appl.* 7 (2017) 014020, <https://doi.org/10.1103/PhysRevApplied.7.014020>.
- [12] C. Wang, K.-J. Jin, Z.-T. Xu, L. Wang, C. Ge, H.-b. Lu, H.-Z. Guo, M. He, G.-Z. Yang, Switchable diode effect and ferroelectric resistive switching in epitaxial  $\text{BiFeO}_3$  thin films, *Appl. Phys. Lett.* 98 (2011) 192901, <https://doi.org/10.1063/1.3589814>.
- [13] C. Ge, K.-J. Jin, C. Wang, H.-B. Lu, C. Wang, G.-Z. Yang, Numerical investigation into the switchable diode effect in metal-ferroelectric-metal structures, *Appl. Phys. Lett.* 99 (2011) 063509, <https://doi.org/10.1063/1.3624849>.
- [14] H. Matsuo, Y. Kitanaka, R. Inoue, Y. Noguchi, M. Miyayama, Switchable diode-effect mechanism in ferroelectric  $\text{BiFeO}_3$  thin film capacitors, *J. Appl. Phys.* (2015)

- 118, <https://doi.org/10.1063/1.4930590>.
- [15] J. Wu, J. Wang, ZnO as a buffer layer for growth of BiFeO<sub>3</sub> thin films, *J. Appl. Phys.* (2010) 108, <https://doi.org/10.1063/1.3460108>.
- [16] S.Y. Yang, J. Seidel, S.J. Byrnes, P. Shafer, C.H. Yang, M.D. Rossell, P. Yu, Y.H. Chu, J.F. Scott, J.W. Ager, L.W. Martin III, R. Ramesh, Above-bandgap voltages from ferroelectric photovoltaic devices, *Nat. Nanotechnol.* 5 (2010) 143–147, <https://doi.org/10.1038/nnano.2009.451>.
- [17] W. Ji, K. Yao, Y.C. Liang, Bulk photovoltaic effect at visible wavelength in epitaxial ferroelectric BiFeO<sub>3</sub> thin films, *Adv. Mater.* 22 (2010) 1763–1766, <https://doi.org/10.1002/adma.200902985>.
- [18] L. Fang, L. You, Y. Zhou, P. Ren, Z. Shihui Lim, J. Wang, Switchable photovoltaic response from polarization modulated interfaces in BiFeO<sub>3</sub> thin films, *Appl. Phys. Lett.* 104 (2014) 142903, <https://doi.org/10.1063/1.4870972>.
- [19] J. Kreisel, M. Alexe, P.A. Thomas, A photoferroelectric material is more than the sum of its parts, *Nat. Mater.* 11 (2012) 260, <https://doi.org/10.1038/nmat3282>.
- [20] C. Paillard, X. Bai, I.C. Infante, M. Guennou, G. Geneste, M. Alexe, J. Kreisel, B. Dkhil, Photovoltaics with ferroelectrics: current status and beyond, *Adv. Mater.* 28 (2016) 5153–5168, <https://doi.org/10.1002/adma.201505215>.
- [21] D. Kim, H. Han, J.H. Lee, J.W. Choi, J.C. Grossman, H.M. Jang, D. Kim, Electron-hole separation in ferroelectric oxides for efficient photovoltaic responses, *Proc. Natl. Acad. Sci. U. S. A.* 115 (2018) 6566–6571, <https://doi.org/10.1073/pnas.1721503115>.
- [22] A. Anshul, H. Borkar, P. Singh, P. Pal, S.S. Kushvaha, A. Kumar, Photoconductivity and photo-detection response of multiferroic bismuth iron oxide, *Appl. Phys. Lett.* 104 (2014) 132910, <https://doi.org/10.1063/1.4870626>.
- [23] A. Anshul, A. Kumar, B.K. Gupta, R.K. Kotnala, J.F. Scott, R.S. Katiyar, Photoluminescence and time-resolved spectroscopy in multiferroic BiFeO<sub>3</sub>: effects of electric fields and sample aging, *Appl. Phys. Lett.* 102 (2013) 222901, <https://doi.org/10.1063/1.4808450>.
- [24] R.K. Katiyar, P. Misra, F. Mendoza, G. Morell, R.S. Katiyar, Switchable photovoltaic effect in bilayer graphene/BiFeO<sub>3</sub>/Pt heterostructures, *Appl. Phys. Lett.* 105 (2014) 142902, <https://doi.org/10.1063/1.4897627>.
- [25] R.K. Katiyar, Y. Sharma, P. Misra, V.S. Puli, S. Sahoo, A. Kumar, J.F. Scott, G. Morell, B.R. Weiner, R.S. Katiyar, Studies of the switchable photovoltaic effect in co-substituted BiFeO<sub>3</sub> thin films, *Appl. Phys. Lett.* 105 (2014) 172904, <https://doi.org/10.1063/1.4900755>.
- [26] Z. Wen, G. Hu, S. Fan, C. Yang, W. Wu, Y. Zhou, X. Chen, S. Cui, Effects of annealing process and MN substitution on structure and ferroelectric properties of BiFeO<sub>3</sub> films, *Thin Solid Films* 517 (2009) 4497–4501, <https://doi.org/10.1016/j.tsf.2008.12.026>.
- [27] H. Xu, Y. Lin, T. Harumoto, J. Shi, C. Nan, Highly (001)-Textured tetragonal BiFeO<sub>3</sub> film and its photoelectrochemical behaviors tuned by magnetic field, *ACS Appl. Mater. Interfaces* 9 (2017) 30127–30132, <https://doi.org/10.1021/acsami.7b07644>.
- [28] X. Yao, C. Wang, S. Tian, Y. Zhou, X. Li, C. Ge, E.-j. Guo, M. He, X. Bai, P. Gao, G. Yang, K. Jin, Growth and physical properties of BiFeO<sub>3</sub> thin films directly on Si substrate, *J. Cryst. Growth* 522 (2019) 110–116, <https://doi.org/10.1016/j.jcrysgro.2019.06.017>.
- [29] J.-s. Wang, K.-j. Jin, H.-z. Guo, J.-x. Gu, Q. Wan, X. He, X.-l. Li, X.-l. Xu, G.-z. Yang, Evolution of structural distortion in BiFeO<sub>3</sub> thin films probed by second-harmonic generation, *Sci. Rep.* 6 (2016) 38268, <https://doi.org/10.1038/srep38268>.
- [30] P. Roy Choudhury, J. Parui, S. Chiniwar, S.B. Krupanidhi, Preferential polarization and its reversal in polycrystalline BiFeO<sub>3</sub>/La<sub>0.5</sub>Sr<sub>0.5</sub>CoO<sub>3</sub> heterostructures, *Solid State Commun* 208 (2015) 15–20, <https://doi.org/10.1016/j.ssc.2015.02.011>.
- [31] V.S. Puli, D.K. Pradhan, R.K. Katiyar, I. Coondoo, N. Panwar, P. Misra, D.B. Chrisey, J.F. Scott, R.S. Katiyar, Photovoltaic effect in transition metal modified polycrystalline BiFeO<sub>3</sub> thin films, *J. Phys. D: Appl. Phys.* 47 (2014) 075502, <https://doi.org/10.1088/0022-3727/47/7/075502>.
- [32] X. Qi, P.-C. Tsai, Y.-C. Chen, Q.-R. Lin, J.-C.-A. Huang, W.-C. Chang, I.-G. Chen, Optimal growth windows of multiferroic BiFeO<sub>3</sub> films and characteristics of ferroelectric domain structures, *Thin Solid Films* 517 (2009) 5862–5866, <https://doi.org/10.1016/j.tsf.2009.03.070>.
- [33] K.Y. Yun, M. Noda, M. Okuyama, Prominent ferroelectricity of BiFeO<sub>3</sub> thin films prepared by pulsed-laser deposition, *Appl. Phys. Lett.* 83 (2003) 3981–3983, <https://doi.org/10.1063/1.1626267>.
- [34] H. Béa, M. Bibes, A. Barthélémy, K. Bouzehouane, E. Jacquet, A. Khodan, J.P. Contour, S. Fusil, F. Wyczisk, A. Forget, D. Lebeugle, D. Colson, M. Viret, Influence of parasitic phases on the properties of BiFeO<sub>3</sub> epitaxial thin films, *Appl. Phys. Lett.* 87 (2005) 072508, <https://doi.org/10.1063/1.2009808>.
- [35] J.K. Kim, S.S. Kim, W.-J. Kim, A.S. Bhalla, R. Guo, Enhanced ferroelectric properties of Cr-doped BiFeO<sub>3</sub> thin films grown by chemical solution deposition, *Appl. Phys. Lett.* 88 (2006) 132901, <https://doi.org/10.1063/1.2189453>.
- [36] Y. Sun, Y. Zhou, H. Liu, Z. Xia, M. Luo, K. Wan, C. Wang, Polarization-controlled leakage current and photovoltaic effect in highly preferentially oriented BiFeO<sub>3</sub> film, *J. Sol-Gel Sci. Technol.* 66 (2013) 429–433, <https://doi.org/10.1007/s10971-013-3028-3>.
- [37] H. Liu, X. Wang, Room temperature saturated polarization in BiFeO<sub>3</sub> film by a simple chemical solution deposition method, *J. Phys. D: Appl. Phys.* 41 (2008) 175411, <https://doi.org/10.1088/0022-3727/41/17/175411>.
- [38] M. Trassin, G.D. Luca, S. Manz, M. Fiebig, Probing ferroelectric domain engineering in BiFeO<sub>3</sub> thin films by second harmonic generation, *Advanced Materials* 27 (2015) 4871–4876, <https://doi.org/10.1002/adma.201501636>.
- [39] A. Kumar, S. Denev, R.J. Zeches, E. Vlahos, N.J. Podraza, A. Melville, D.G. Schlom, R. Ramesh, V. Gopalan, Probing mixed tetragonal/rhombohedral-like monoclinic phases in strained bismuth ferrite films by optical second harmonic generation, *Appl. Phys. Lett.* 97 (2010) 112903, <https://doi.org/10.1063/1.3483923>.
- [40] S. Tian, C. Wang, Y. Zhou, X. Li, P. Gao, J. Wang, Y. Feng, X. Yao, C. Ge, M. He, X. Bai, G. Yang, K. Jin, Manipulating the ferroelectric domain states and structural distortion in epitaxial BiFeO<sub>3</sub> ultrathin films via bi nonstoichiometry, *ACS Appl. Mater. Interfaces* 10 (2018) 43792–43801, <https://doi.org/10.1021/acsami.8b15703>.
- [41] L. Wang, K.-j. Jin, C. Ge, C. Wang, H.-z. Guo, H.-b. Lu, G.-z. Yang, Electro-photo double modulation on the resistive switching behavior and switchable photoelectric effect in BiFeO<sub>3</sub> films, *Appl. Phys. Lett.* 102 (2013) 252907, <https://doi.org/10.1063/1.4812825>.
- [42] L. Li, Y. Zhang, L. Xie, J.R. Jokisaari, C. Beekman, J.C. Yang, Y.H. Chu, H.M. Christen, X. Pan, Atomic-scale mechanisms of defect-induced retention failure in ferroelectrics, *Nano Lett* 17 (2017) 3556–3562, <https://doi.org/10.1021/acs.nanolett.7b00696>.
- [43] A. Singh, Z.R. Khan, P.M. Vilarinho, V. Gupta, R.S. Katiyar, Influence of thickness on optical and structural properties of BiFeO<sub>3</sub> thin films: pld grown, *Mater. Res. Bull.* 49 (2014) 531–536, <https://doi.org/10.1016/j.materresbull.2013.08.050>.
- [44] J.F. Ihlefeld, N.J. Podraza, Z.K. Liu, R.C. Rai, X. Xu, T. Heeg, Y.B. Chen, J. Li, R.W. Collins, J.L. Musfeldt, X.Q. Pan, J. Schubert, R. Ramesh, D.G. Schlom, Optical band gap of BiFeO<sub>3</sub> grown by molecular-beam epitaxy, *Appl. Phys. Lett.* 92 (2008) 142908, <https://doi.org/10.1063/1.2901160>.
- [45] J.H. Lee, J.H. Jeon, C. Yoon, S. Lee, Y.S. Kim, T.J. Oh, Y.H. Kim, J. Park, T.K. Song, B.H. Park, Intrinsic defect-mediated conduction and resistive switching in multiferroic BiFeO<sub>3</sub> thin films epitaxially grown on SrRuO<sub>3</sub> bottom electrodes, *Appl. Phys. Lett.* 108 (2016) 112902, <https://doi.org/10.1063/1.4944554>.
- [46] G.-L. Yuan, J. Wang, Evidences for the depletion region induced by the polarization of ferroelectric semiconductors, *Appl. Phys. Lett.* 95 (2009) 252904, <https://doi.org/10.1063/1.3268783>.
- [47] F. Yan, G. Chen, L. Lu, J.E. Spanier, Dynamics of photogenerated surface charge on BiFeO<sub>3</sub> films, *ACS Nano* 6 (2012) 2353–2360, <https://doi.org/10.1021/nn204604m>.
- [48] A.B. Swain, M. Rath, P.P. Biswas, M.S.R. Rao, P. Murugavel, Polarization controlled photovoltaic and self-powered photodetector characteristics in Pb-free ferroelectric thin film, *APL Mater* 7 (2019) 011106, <https://doi.org/10.1063/1.5064454>.